Blocking M2-Like Macrophage Polarization Using Decoy Oligodeoxynucleotide-Based Gene Therapy Prevents Immune Evasion for Pancreatic Cancer Treatment

Chang-Jung Chen[1], Hao-Chen Wang[1,2,3], Ya-Chin Hou[1,4], Yi-Ying Wu[1,4], Chi-Chang Shieh[1,5], and Yan-Shen Shan[1,3,6]

ABSTRACT

M2-like macrophages exhibit immunosuppressive activity and promote pancreatic cancer progression. Reactive oxygen species (ROS) affect macrophage polarization; however, the mechanism remains unclear. This study aimed to elucidate the underlying molecular basis and design a gene therapy to inhibit M2-like polarization. Microarray analysis and immunofluorescence staining were performed in M1-like and M2-like macrophages to ascertain the expression of *CYBB*, a major intracellular ROS source. Coculture assay and syngeneic orthotopic pancreatic cancer mice models were used to study the mechanism of M2-like skewing. Decoy oligodeoxynucleotides (ODNs) were designed to manipulate CYBB transcription to inhibit M2-like polarization and control tumor growth. Lipopolysaccharide treatment polarized U937 cells to M1-like macrophages in which CYBB expression was increased. In contrast, coculture with PANC-1 cells induced M2-like polarization in U937 cells with CYBB downregulation. High CD204 M2-like expression in combination with low CYBB expression was associated with the worst prognosis in patients with pancreatic cancer. STAT6 and HDAC2 in U937 cells were activated by cancer cell–derived IL4 after coculture and then bound to the *CYBB* promoter to repress CYBB expression, resulting in M2-like polarization. Diphenyleneiodonium, 8λ^3-iodatricyclo[7.4.0.0^{2,7}]trideca-1(13),2,4,6,9,11-hexaen-8-ylium chloride that inhibits ROS production could block this action. Knockdown of STAT6 and HDAC2 also inhibited M2-like polarization and maintained the M1-like phenotype of U937 cells after coculture. Decoy ODNs interrupting the binding of STAT6 to the *CYBB* promoter counteracted M2-like polarization and tumor growth and triggered antitumor immunity *in vivo*. Gene therapy using STAT6-*CYBB* decoy ODNs can inhibit M2-like polarization, representing a potential therapeutic tool for pancreatic cancer.

Introduction

The tumor microenvironment (TME) is a dynamic and complex milieu surrounding the tumor, which plays a critical role in regulating cancer progression and affecting therapeutic outcomes (1). The TME contains not only tumor cells but also diverse cell types, such as Th1, Th2, B lymphocytes, tumor-associated macrophages (TAMs), dendritic cells, natural killer (NK) cells, neutrophils, myeloid-derived suppressor cells, and fibroblasts (2). Among them, TAMs represent the prominent immune cell type, capable of suppressing the innate and adaptive immunity, assisting tumor cells in evading immune attack, and supporting tumors inclined toward cold tumors (3, 4). In pancreatic cancer, TAMs are the most abundant immune cells infiltrating the TME, which orchestrate tumor-promoting inflammation, and have been associated with a poor prognosis (5, 6).

Past studies have shown that macrophages are a diverse group of immune cells with different properties and functions that may originate from distinct cell differentiation pathways and environments (7). The macrophage plasticity in different states of macrophage activation has been proposed, like M1-like, M2a-alternative, M2b-type 2, M2c-deactivated, and M2d (8). Furthermore, it is well known that M1-like macrophages with antitumor activity produce inflammatory cytokines such as IFNγ, CCL2, IL1β, IL12p40, and reactive nitrogen and oxygen species (RNS and ROS) to promote Th1 responses and increase antimicrobial ability against various types of bacteria and viruses (9, 10). Macrophages with M2-like phenotype exhibit protumor activity and release TGFβ, VEGFA, CCL17, and CCL21 to exert anti-inflammatory effects (9, 10). Considerable evidence has indicated that M2-like TAMs exert immunosuppressive effects by secreting various chemokines, cytokines, and enzymes to downregulate immune cells activation (11). For example, M2-like TAMs can secret IL10 to activate regulatory T cells that suppress the killing effect of T and NK cells (12). In addition to soluble inhibitory molecules, M2-like TAMs reportedly express well-known immune checkpoint proteins to negatively regulate immune responses, such as classical and nonclassical MHC class I molecules, cytotoxic T-lymphocyte antigen 4 ligands, and

[1]Institute of Clinical Medicine, College of Medicine, National Cheng Kung University, Tainan, Taiwan. [2]Medical Imaging Center, Innovation Headquarters, National Cheng Kung University, Tainan, Taiwan. [3]Comparative Medicine Center, Innovation Headquarters, National Cheng Kung University, Tainan, Taiwan. [4]Clinical Medicine Research Center, National Cheng Kung University Hospital, College of Medicine, National Cheng Kung University, Tainan, Taiwan. [5]Division of Allergy, Immunology and Rheumatology, Department of Pediatrics, National Cheng Kung University Hospital, National Cheng Kung University, Tainan, Taiwan. [6]Department of Surgery, National Cheng Kung University Hospital, College of Medicine, National Cheng Kung University, Tainan, Taiwan.

C.-C. Shieh and Y.-S. Shan contributed equally to this article.

Corresponding Author: Yen-Shen Shan, Division of General Surgery, Department of Surgery, National Cheng Kung University Hospital, College of Medicine, National Cheng Kung University Institute of Clinical Medicine, College of Medicine, National Cheng Kung University 138, Sheng-Li Road, Tainan 70428, Taiwan. E-mail: ysshan@mail.ncku.edu.tw

Mol Cancer Ther 2024;23:1431–45

doi: 10.1158/1535-7163.MCT-23-0767

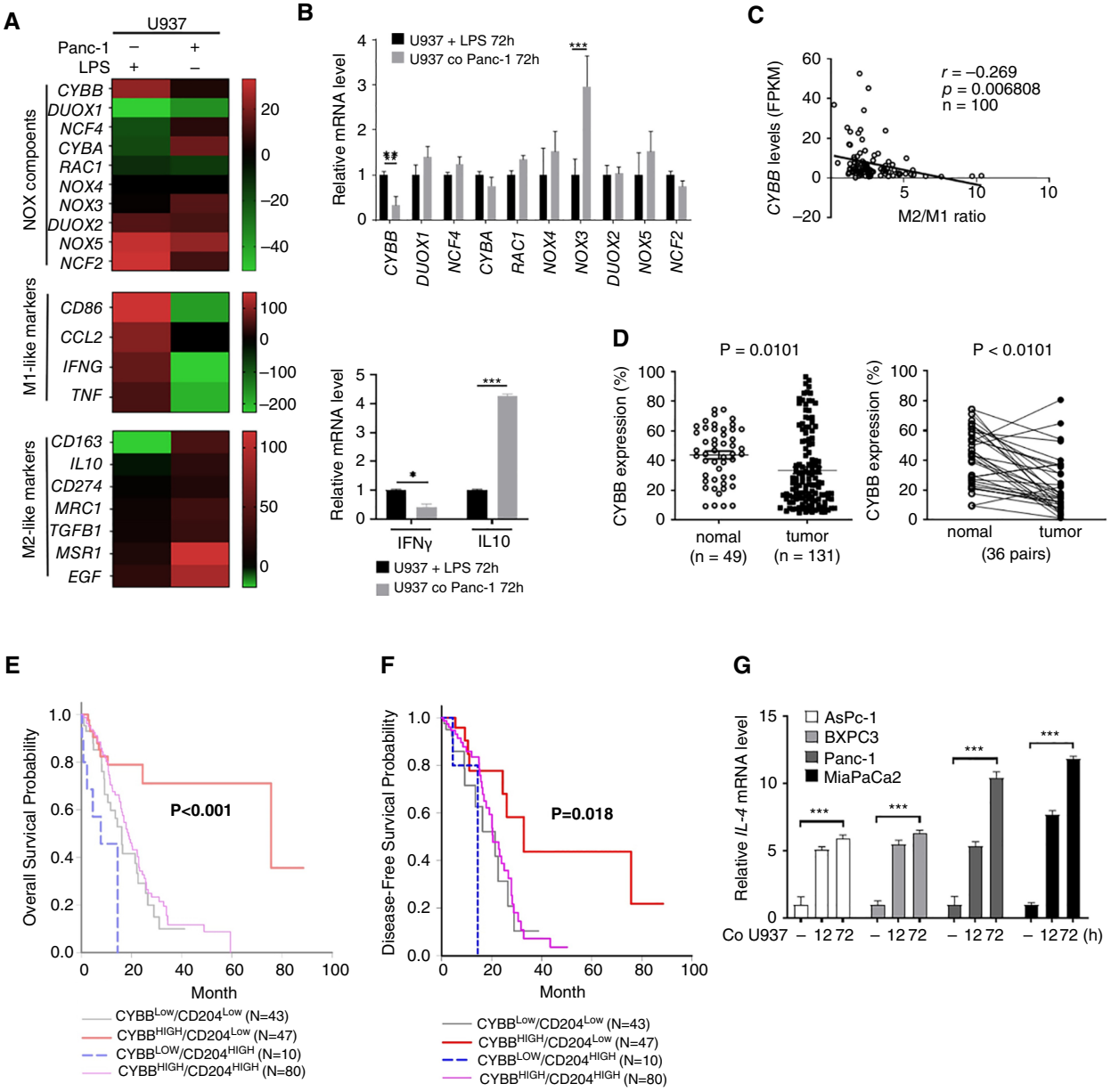

Figure 1.

CYBB affects macrophage polarization, patient outcomes, and IL4 stimulation in the TME. **A,** The heatmap of differentially expressed genes of NOX components and M1-like/M2-like macrophage markers expression in U937 cells treated with LPS or cocultured with PANC-1 cells for 72 hours. **B,** RT-qPCR showed that *CYBB* mRNA expression decreased significantly and M1-like/M2-like mRNA expression significantly changed after coculture with PANC-1 cells for 72 hours. The bar graphs depict relative mRNA expression. **, $P < 0.01$; ***, $P < 0.001$. Data represent the mean of three independent experiments. **C,** Correlation analysis between *CYBB* expression and M2-like/M1-like ratio (CD204/CD86) was performed using our RNAseq data (FPKM values) of 100 pancreatic tumors. Pearson correlation coefficient (*r*) and significance level (*P* value) are shown for correlation. **D,** CYBB level was examined in pancreatic cancer tissue and normal tissue ($P = 0.01$) and in 36 matched pairs of pancreatic tumors and adjacent nontumor tissue ($P < 0.0001$). **E** and **F,** The Kaplan–Meier survival curves compared DFS and OS of patients stratified based on $CD204^+$ M2-like TAMs infiltration and CYBB expression. *P* values were determined using the log-rank test. **G,** RT-qPCR analysis of *IL4* level was performed in U937 cells cocultured with different pancreatic cell lines. The bar graphs depict relative mRNA expression. ***, $P < 0.001$, significant differences between groups. Data represent the mean of three independent experiments. **H** and **I,** U937 cells were (*Continued on the following page.*)

programmed cell death protein ligand 1 (PD-L1; refs. 13, 14). Therefore, blocking of immune checkpoints is considered a promising approach for activating therapeutic antitumor immunity (15).

Reactive oxygen species (ROS) are the most common oxygen radicals in the body, such as superoxide, hydroxide, and nonradicals (16). Much research has shown that ROS, specifically

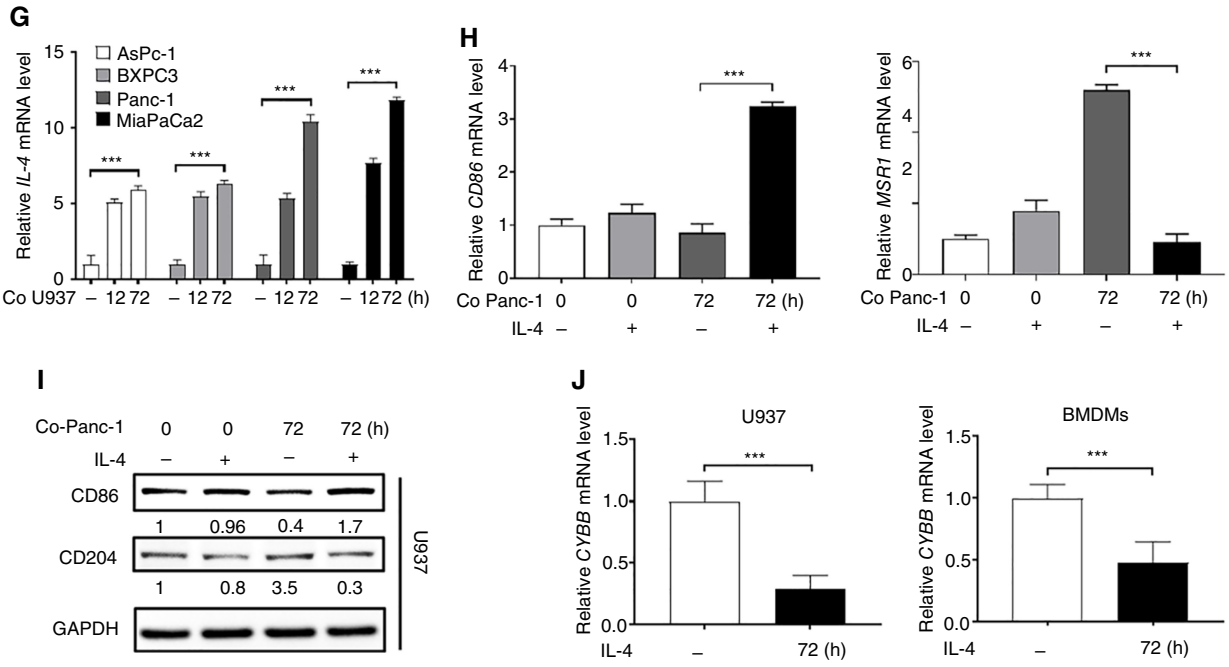

Figure 1.
(*Continued*.) cocultured with PANC-1 cells and simultaneously treated with IL4 neutralizing antibody. After 72 hours of incubation, U937 cells were collected for Western blotting to measure M1/M2 markers, CYBB, and GAPDH protein expression and RT-qPCR of M1-like (CD86) and M2-like (MSR1/CD204) markers mRNA level. **J,** RT-qPCR analysis of *CYBB* expression in U937 cells treated with IL4 (20 ng/mL) for 72 hours. The bar graphs depict relative mRNA expression. ***, $P < 0.001$, compared with control. Data represent the mean of three independent experiments.

produced by the NADPH oxidase complex (NOX, also called Cybb or gp91phox), are a critical factor impacting host defense and cell differentiation in multicellular organisms (17). NOX2 is the major isoform of NOX in phagocytes and dendritic cells. NOX2, p22phox, p67phox, p47phox, p40phox, and Rac can form active enzyme complexes to produce ROS. Among the six subunits, gp91phox and p22phox are membrane proteins mainly constituting the flavin cytochrome b558 (cyt b558) and the catalytic core (17, 18). A recent report showed that an antioxidant drug, butylated hydroxyanisole, efficiently suppressed monocyte–macrophage differentiation, the occurrence, and tumorigenesis in a mouse cancer model, suggesting that ROS are essential for the formation (19).

To date, targeting the signaling pathways such as CCL2-CCR2, CSF1-CSF1R, CD47-SIRPα, and CXCL12-CXCR4 has therapeutic potential to limit monocyte recruitment, reduce the activation of M2-like TAMs, and reverse the M2-like phenotype to the antitumor M1-like phenotype (10, 20–22); however, the systemic adverse effects of these treatments have been a challenging issue. For example, blocking CCL2-CCR2 signaling that drives the recruitment of circulating inflammatory monocytes to inflammatory centers can reduce TAM population at primary and metastatic sites (21, 23, 24). However, a previous clinical trial for pancreatic cancer has shown that treatment with the small molecule CCR2 inhibitor, PF-04136309 decreased $CD14^+CCR2^+$ inflammatory monocytes in the peripheral blood and TAMs formation in the TME, but this was accompanied by severe side effects such as pulmonary toxicity, dysesthesia, diarrhea, and hypokalemia (23, 25). To solve this problem, using double-stranded "decoy" oligonucleotides to target the action of transcription factors (TFs) is a promising alternative approach because of their good tolerance and low toxicity (26–28). Therefore, the objective of this study was to investigate the mechanism underlying M2 polarization and design decoy oligodeoxynucleotide (ODN)-based gene therapy to reduce M2-like formation and reactivate antitumor immunity for pancreatic cancer treatment.

Materials and Methods

Reagents

Diphenyleneiodonium, 8λ³-iodatricyclo[7.4.0.0²,⁷]trideca-1(13),2,4,6,9,11-hexaen-8-ylium chloride (DPI; Sigma-Aldrich; D2926; ref. 29) was used to treat cells at a concentration of 5 μmol/L for 24 hours. Lipopolysaccharide (LPS; Sigma-Aldrich; L2387; ref. 30) was used to treat cells at a concentration of 100 nmol/L for 24 hours. IL4-neutralizing antibodies (GeneTex; GTX15760; clone name: 25D2; RRID: AB_3099661) were used at 1 mg/mL for 72 hours (31). IL4 recombinant protein (proteintech; Cat No: HZ-1004) was used at a concentration of 20 ng/mL at various time points (32). The following concentrations of drugs were used to pretreat cells for 24 hours: Ruxolitinib, (R)-3-(4-(7H-pyrrolo[2,3-d]pyrimidin-4-yl)-1H-pyrazol-1-yl)-3-cyclopentylpropanenitrile (Rux; Cat No: S1378; ref. 33) at 10 μmol/L; Tofacitinib, 3-[(3R,4R)-4-methyl-3-[methyl(7H-pyrrolo[2,3-d]pyrimidin-4-yl)amino]piperidin-1-yl]-3-oxopropanenitrile (Tof; Cat No: S2789; ref. 34) at 50 μmol/L; AS1517499, 4-(benzylamino)-2-[2-(3-chloro-4-hydroxyphenyl)ethylamino] pyrimidine-5-carboxamide (AS; Cat No: S8685; ref. 35) at 250 nmol/L; Trichostatin A, (2E,4E,6R)-7-[4-(dimethylamino)phenyl]-N-hydroxy-4,6-dimethyl-7-oxohepta-2,4-dienamide (TSA; Cat No: S1045; ref. 36) at 10 μmol/L; and LBH589, (E)-N-hydroxy-3-[4-[[2-(2-methyl-1H-indol-3-yl)ethylamino]methyl]phenyl]prop-2-enamide (LBH; Cat

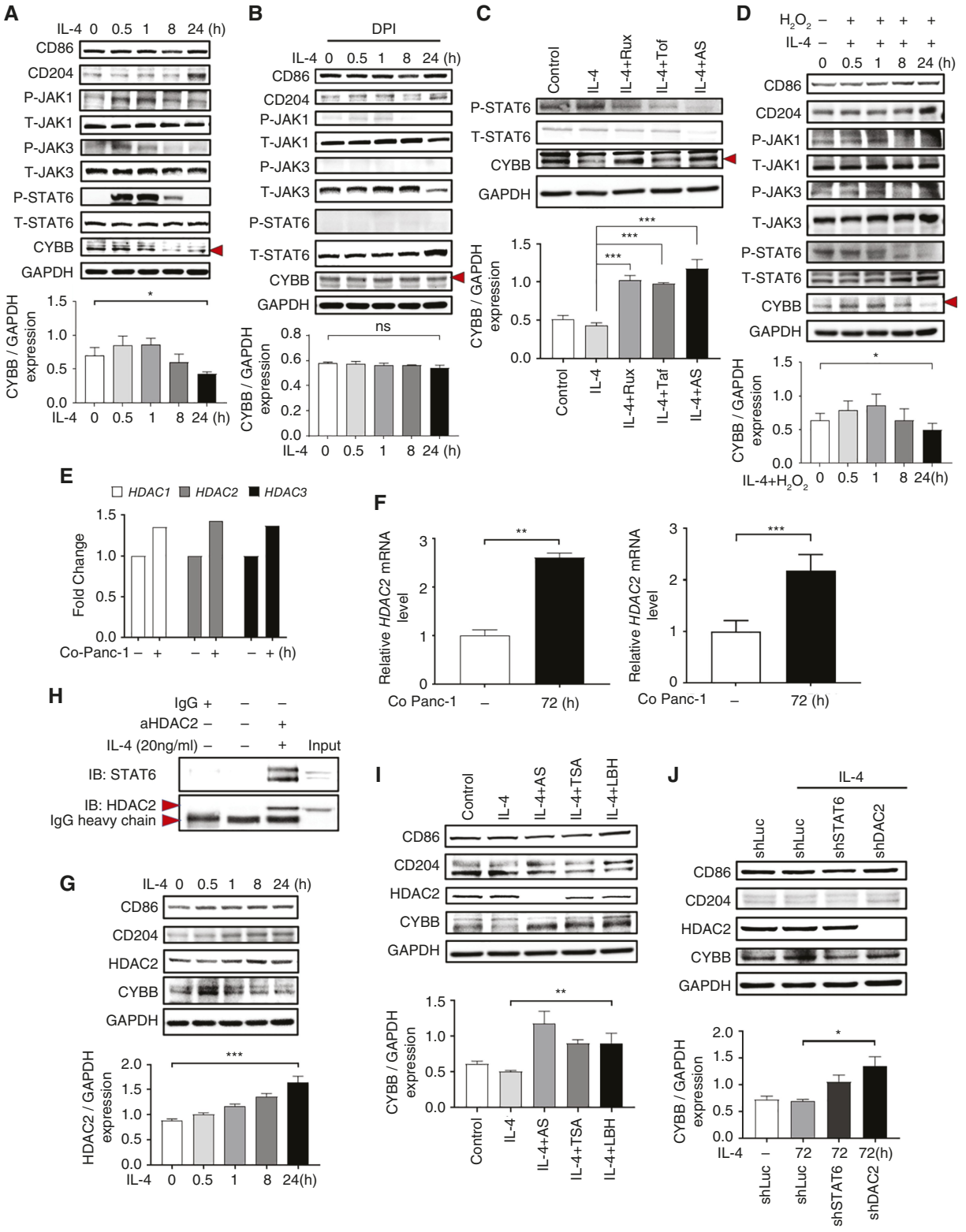

Figure 2.

JAK/STAT6/HDAC2 is the downstream signaling of IL4 in regulating CYBB expression. **A,** Time-dependent effect of IL4 (20 ng/mL) on JAK1, JAK3, STAT6, and CYBB protein expression. The bar graphs depict relative protein expression. *, $P < 0.05$, compared with control. GAPDH was used as a loading control. The bar graph depicts the ratio of CYBB/GAPDH. *, $P < 0.05$, compared to 0 hours treated with IL4 treatment. Data represents (*Continued on the following page.*)

No: S11030; ref. 37) at 50 μmol/L. All drugs were purchased from Selleckchem.

Cell line and culture conditions

The human pancreatic cancer cell lines AsPC-1 (Catalog No. CRL-1682; RRID: CVCL_0152), BxPC3 (Catalog No. CRL-1687; RRID: CVCL_0186), PANC-1 (Catalog No. CRL-1469; RRID: CVCL_0480), and MiaPaCa2 (Catalog No. CRL-1420; RRID: CVCL_0428), and the monocytic U937 (Catalog No. CRL-1593.2; RRID: CVCL_0007), and THP-1 (Catalog No. TIB-202; RRID: CVCL_0006) cell lines were obtained from the American Type Culture Collection (ATCC) and have been validated by the Center for Genomic Medicine, National Cheng Kung University (NCKU), using the ATCC short tandem repeat database. The mouse pancreatic cancer cell line KPC was established from *Pdx1-Cre*; $Kras^{G12D/+}$; $Trp53^{-/-}$ mice kindly gifted by Dr. Kuang-Hung Cheng (Institute of Biomedical Sciences, National Sun Yat-sen University, Kaohsiung, Taiwan). KPC cells were transfected with the pGL4 Luciferase Reporter plasmid to establish a stable luciferase-expressing clone, KPC^{LUC}. All cells were cultured in RPMI 1640 medium (Hyclone; SH30027.02) supplemented with 10% fetal bovine serum (Hyclone; SH30071.03), 2 mmol/L L-glutamine (Simply; Cat. No CC515-0100), 100 units/mL Antibiotic-Antimycotic (Simply; Cat. No CC501-0100), and 1 mol/L HEPES (Simply; Cat. No CC519-0100) at 37°C in a humidified atmosphere of 5% CO_2. All cell lines were routinely detected for the presence of mycoplasma using the Mycoplasma Detection Kit (BioSmart, BSMP-101) performed every 6 months.

Gene expression microarray and analysis

We collected U937 cells after 72 hours of LPS treatment or 72 hours of coculture with PANC-1 cells for microarray analysis and submitted them to the Gene Expression Omnibus database (GSE269815). The gene microarray data were analyzed using the Agilent Human whole genome oligo 4*44k chip (array kit serial number: US00082833) and Agilent's gene expression microarray software, including Feature Extraction and GeneSpring GX. Feature Extraction software extracts data from microarray images and provides workflows for analysis. GeneSpring GX offers statistical tools for data analysis and visualization (Welgene Biotech), and the genes of interest were drawn as a heatmap.

In vitro coculture assay

U937 cells were seeded into cell culture transwell inserts (3×10^5 cells per insert) with pore size of 0.4 μm (Falcon) packed in a six-well plate (GeneDireX), where PANC-1 cells were grown (3×10^5 cells per well). The cocultures were incubated at 37°C for 72 hours.

The differentiation of macrophages from murine bone marrow cells

Bone marrow cell suspensions were separated by flushing femurs and tibias of 8 to 12 weeks old wild-type mice with complete RPMI1640 media. Pipetting dislodged aggregates, and debris was removed using a 70 μm nylon web. Cells were washed using HBSS, adjusted to a 10^6 cells/mL suspension, and seeded on 10 cm low attachment surface dishes. Cells were treated with 20 ng/μL rmM-CSF (PeproTech, 315-03) and maintained in a humidified incubator at 37°C and 5% CO_2.

RNA sequencing

RNA sequencing (RNA-seq) of 100 pancreatic tumors was conducted and the data were analyzed by Allbio Life Co., Ltd. We evaluated the correlation between CYBB expression and the M2 (CD204)/M1 (CD86) ratio using their FPKM values.

Decoy ODN treatment in syngeneic orthotopic mouse models of pancreatic cancer

The experimental protocols and procedures for the animal study were approved by the Institutional Animal Care and Use Committee of NCKU (IACUC No.: 103150 and 110331). Luciferase-expressing KPC cells (KPC^{LUC}, 1×10^7 cells in 50 μL serum-free medium) were orthotopically injected into the pancreas of 8 to 12 weeks old male C57BL/6 mice. Two weeks after the cancer cell injection, the tumor-bearing mice were treated with decoy ODNs (1 μg/mL in normal saline, intravenously) once weekly for 3 weeks.

Immunohistochemistry

Paraffin-embedded sections were deparaffinized and antigens were unmasked by autoclaving at 121°C for 10 minutes in sodium citrate buffer (10 mmol/L; pH 6.0). Sections were incubated with primary antibodies at 4°C overnight, followed by incubation with secondary antibodies at room temperature for 30 minutes. Immunoreactivity was visualized using the DAB chromogen system (DAKO). Information regarding the antibodies and their dilution ratios used in this study is shown in Supplementary Table S1.

Immunofluorescence staining

After approval from the Institutional Review Board of NCKU Hospital, a pancreatic cancer tissue microarray (TMA) was constructed from paraffin-embedded blocks of 187 patients with pancreatic cancer resected at NCKU Hospital. TMA paraffin blocks

(*Continued*.) the mean of three independent experiments. **B,** The time-dependent effect of DPI (5 μmol/L) and IL4 (20 ng/mL) treatment on JAK1, JAK3, STAT6, and CYBB protein expression. The bar graph depicts the ratio of CYBB/GAPDH. ns, not significant, compared to 0 hour. Data represent the mean of three independent experiments. **C,** U937 cells were pretreated with JAK1 (Rux, 10 μmol/L), JAK3 (Tof, 50 μmol/L), and STAT6 (AS1517499, 250 nmol/L) inhibitors for 24 hours and then treated with IL4 (20 ng/mL) for 1 hour by Western blot analysis. The bar graph depicts the ratio of CYBB/GAPDH. ***, $P < 0.001$, compared with IL4 treatment without inhibitors control. Data represent the mean of three independent experiments. **D,** The time-dependent effect of H_2O_2 (100 nmol/L) treatment on JAK1, JAK3, STAT6, and CYBB protein expression. The bar graph depicts the ratio of CYBB/GAPDH. *, $P < 0.05$, compared to 0 hour. Data represents the mean of three independent experiments. **E,** Microarray analysis of *HDACs* gene expression in U937 cells after coculture with PANC-1 cells for 72 hours. **F,** RT-qPCR analysis of *HDAC2* gene expression in U937 cells cocultured with pancreatic cancer cells. The bar graphs depict relative mRNA expression. **, $P < 0.01$; compared with control. **G,** Time-dependent IL4 (20 ng/mL) effect in U937 cells on HDAC2 and CYBB protein expression. The bar graph depicts the ratio of CYBB/GAPDH. ***, $P < 0.001$, compared with IL4 treatment. Data represent the analysis of three independent experiments. **H,** The co-immunoprecipitation protein analysis of 20 ng/mL IL4 treatment and against HDAC2 antibody in U937 cells, then the interaction between STAT6 and HDAC2 protein expression. **I,** U937 cells were pretreated STAT6 (AS1517499, 250 nmol/L) and HDAC (TSA, 10 μmol/L; LBH589, 50 μmol/L) inhibitors for 24 hours followed by IL4 (20 ng/mL) for 1 hour. Cell lysates were subjected to Western blotting. The bar graph depicts the ratio of CYBB/GAPDH. **, $P < 0.01$, compared with IL4 treatment without inhibitors control. Data represent the mean of three independent experiments. **J,** shSTAT6 or shHDAC2 U937 cells were treated with IL4 (20 ng/mL) for 1 hour. Cell lysates were subjected to Western blotting. The bar graph depicts the ratio of CYBB/GAPDH. *, $P < 0.05$, compared with IL4 treatment. Data represent the mean of three independent experiments.

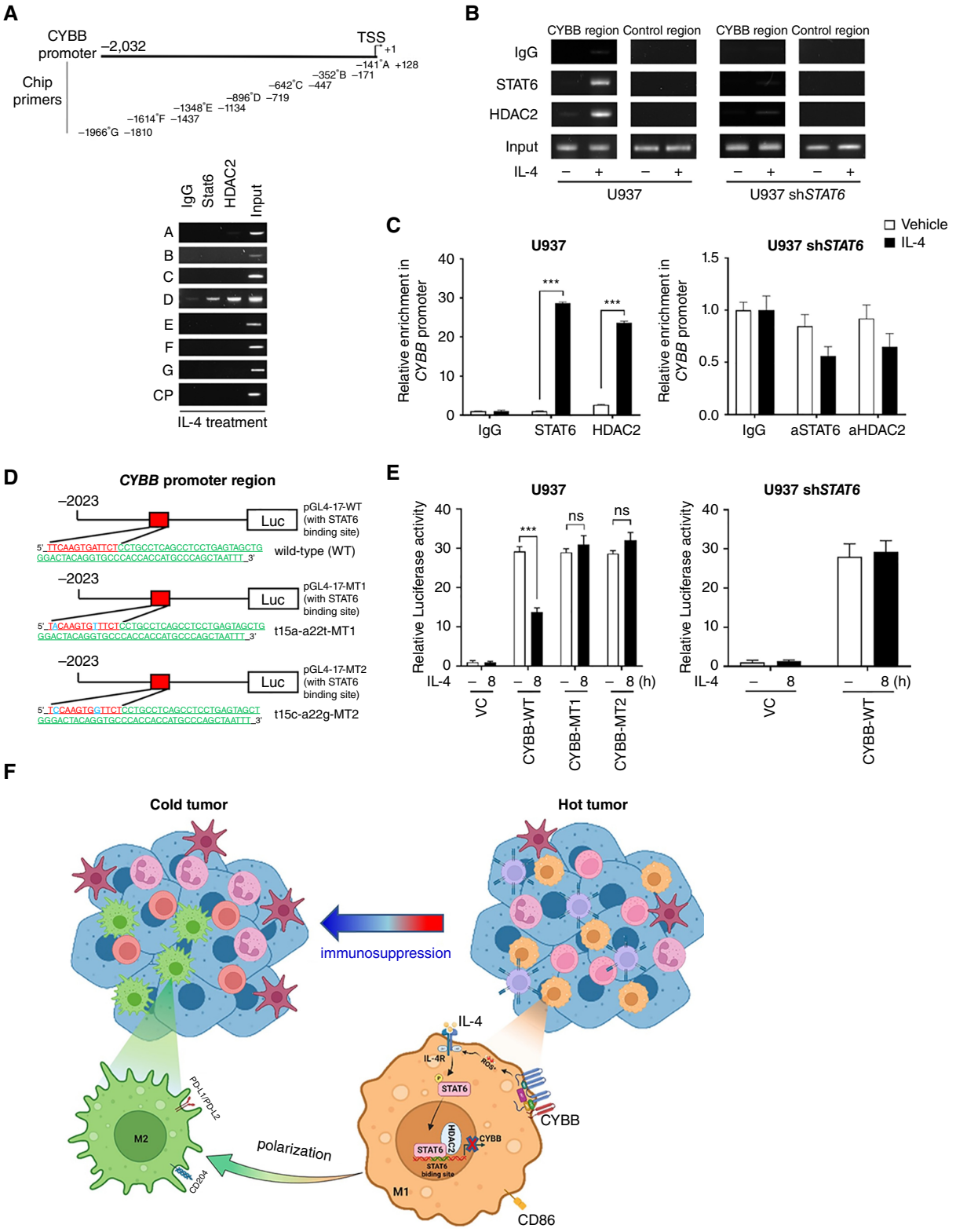

Figure 3.

Both STAT6 and HDAC2 bind to the *CYBB* promoter. **A,** Schematic representation showing the PCR primer design for the *CYBB* promoter region used in this study. U937 cells were exposed to IL4 for 1 hour, and ChIP assay was performed using antibodies against STAT6 and HDAC2 and negative control IgG antibodies. The PCR products were amplified from the final DNA extraction using different pairs of primers on the *CYBB* promoter (*Continued on the following page.*)

were cut into 5 μm sections. TMA sections were stained with primary antibodies at 4°C overnight followed by incubation with fluorescent-conjugated secondary antibodies at room temperature for 1 hour. The nuclei were stained with 4,6-diamidino-2-phenylindole (DAPI). Panoramic images of immunofluorescence (IF)-stained TMAs were acquired using the FACS-like Tissue Cytometry System (Tissue Gnostics, Vienna, Austria). The percentage of stained cells was quantified using the TissueQuest system software TissueFAX (Tissue Gnostics, Vienna, Austria). Information regarding the antibodies and their dilution ratios used in this study is shown in Supplementary Table S1.

RNA isolation and quantitative PCR

Total RNA was isolated from the cultured cells using TRIzol (Invitrogen). The purity and concentration of the RNA were determined using a Nanodrop spectrophotometer (Thermo Fisher Scientific; ND-1000). Total RNA from each sample was reverse transcribed into 2 μg cDNA using Deoxyt HiSpec Reverse Transcriptase (Yeastern Biotech). Quantitative assessment of mRNA levels was performed by qPCR using KAPA qPCR SYBR Green Master Mix (KAPA) on a StepOne Real-Time PCR System (Applied Biosystems). The reaction conditions were as follows: initial denaturation at 95°C for 5 minutes; 40 cycles of denaturation at 95°C for 10 seconds; and annealing at 60°C for 10 seconds. mRNA expression was determined using the $2^{-\Delta\Delta Ct}$ method (fold difference) and normalized to that of GAPDH. The sequences of the human and mouse primers used in this study are listed in Supplementary Table S2.

Lentiviral-based stable cell line generation

STAT6, *HDAC2*, and nontarget short hairpin RNA (shRNA) vectors were purchased from the National RNAi Core Facility, Academia Sinica, Taipei, Taiwan. Lentiviral transfection of U937 cells with shRNAs was performed in the presence of 8 μg/mL polybrene (Sigma-Aldrich, AL-118). Puromycin (P9620; Sigma-Aldrich) was used to select permanent cell lines.

Western blotting analysis

The harvested cells were washed twice with PBS and lysed in ice-cold radioimmunoprecipitation assay (RIPA) lysis buffer (Millipore) for 30 minutes. Lysates were cleared by centrifugation at 14,000 rpm for 10 minutes at 4°C, and the protein concentration was measured using the Bradford assay (Bio-Rad Laboratories, 500-0006). For Western blot analysis, cell lysates were boiled for 5 minutes in sample buffer before being resolved on SDS-polyacrylamide gels. After separation, the proteins were transferred to the PVDF membranes (Millipore, IPVH00010). The membrane was blocked with 5% nonfat dried milk in TBST buffer (20 mmol/L Tris-HCL, pH 7.4, 150 mmol/L NaCl, 0.1% Tween 20) for 1 hour and then incubated overnight at 4°C with specific primary antibodies. Subsequently, the membrane was washed with TBST and incubated with horseradish peroxidase–conjugated secondary antibodies (LEADGENE) for 1 hour at room temperature. The blot signals were developed using an enhanced chemiluminescence kit (GeneTex, GTX14698) and captured using the iBright 1000 Series Image System (Thermo Fisher). Information regarding the antibodies and their dilution ratios used in this study is shown in Supplementary Table S1.

Chromatin immunoprecipitation

According to the manufacturer's protocol, chromatin immunoprecipitation (ChIP) was performed using the EZ-ChIP Chromatin Immunoprecipitation Kit (Millipore). Briefly, the cells were fixed with 1% formaldehyde for 15 minutes, and unreacted formaldehyde was quenched by adding 125 mmol/L glycine for 15 minutes. Chromatin was sonicated to an average length of 200 to 1,000 bp. Samples were reacted with anti-STAT6 (1:50, Cell Signaling Technology, #5397S) and anti-HDAC2 (1:50, Cell Signaling Technology, #57156S). The DNA sample precipitated with the target antibody was detected by PCR using the primers covering the −896/−719 region of the *CYBB* promoter: forward 5′- TGACACAATCTCGGC TCACTGCAA-3′ and reverse 5′-TCACGCCTGTAATCCCAGCAC TTT-3′.

Luciferase reporter assay

The *CYBB*-WT– and *CYBB*-mutated reporter constructs were generated by standard gene synthesis and cloning of the promoter sequences in the luciferase reporter system (pGL4.17 vector, Promega). U937 cells were transfected with the above reporter plasmids using electroporation (NEPA21 electroporator). Cells (1×10^6) were suspended in OPTI-MEM (100 μL) and mixed with 10 μg plasmid DNA in an electrode chamber. Twenty-four hours after transfection, cells were stimulated with or without IL4 for 8 hours, and then were harvested and lysed for luciferase and Renilla measurements using the Dual-Luciferase Assay System (Promega). To assess transfection efficiency, cotransfection with the pRL-TK vector as an internal control allowed normalization of transfection by Renilla luciferase activity.

Synthesis of STAT6-*CYBB* decoy ODN

The decoy ODNs were synthesized by Genomics (New Taipei City, Taiwan). STAT6-*CYBB* decoy ODNs, mutated decoy ODNs, and scrambled ODNs were synthesized using selected sequence targets (38, 39). The STAT6-*CYBB* decoy ODN is a double-stranded phosphonothioate 28mer DNA that acts as an antagonistic inhibitor of the TF STAT6 and binding site of consensus sequence is underlined. We designed the sequences to act as a signal-strand DNA as follows: STAT6-*CYBB* decoy ODN, 5′-CTGACTCCC-AGGTTCAAGTGATTCTCCT-3′ and 3′ -GACTGAGGGTCCAAG-TTCACTAAGAGGA-5′; mutated decoy ODN, 5′-CTGACTCCC-GAGTTCAAGTGATTCCCCT-3′ and 3′-GACTGAGGGCTCAAG-TTCACTAAGGGGA-5′; scrambled decoy ODN, 5′-CGAAAATTC-GTTAAATCACTAGCTTACC-3′ and 3′-GCTTTTAAGCAATTT-AGTGATCGAATGG-5′. Synthetic ODNs were dissolved in sterile annealing buffer (100 mmol/L Tris-HCl pH 7.5, 10 mmol/L EDTA pH 8.0, 1 mol/L NaCl, and ddH_2O) and were annealed for 3 hours

(*Continued*.) region. **B** and **C,** U937 cells and sh*STAT6*-U937 cells were treated with IL4 (20 ng/mL) for 1 hour followed by the ChIP assay. The PCR and RT-qPCR products from primer **D** were performed to confirm data. The bar graphs depict the relative expression of RT-qPCR products. ***, $P < 0.001$, significant differences between groups. Data represent the mean of three independent experiments. **D,** Schematic representation showing the *CYBB*-WT reporter with the *CYBB* promoter containing a wild-type STAT6 binding site and the *CYBB*-MT1 and MT2 reporters with the *CYBB* promoters in which the STAT6 binding site was mutated. **E,** U937 cells and shSTAT6 U937 cells were electroporated with the pRL-TK reporter in combination with the *CYBB*-WT reporter, the *CYBB*-MT1 reporter, the *CYBB*-MT2 reporter, or vector control (VC). After 24 hours of electroporation, cells were treated with IL4 (20 ng/mL) for 8 hours, and luciferase activity was detected by the dual luciferase assay. The bar graphs depict relative luciferase activity. ***, $P < 0.001$, significant differences between groups. Data represent the mean of three independent experiments. **F,** Schematic conclusion showing the detailed mechanism elucidating the role of CYBB in M2 polarization.

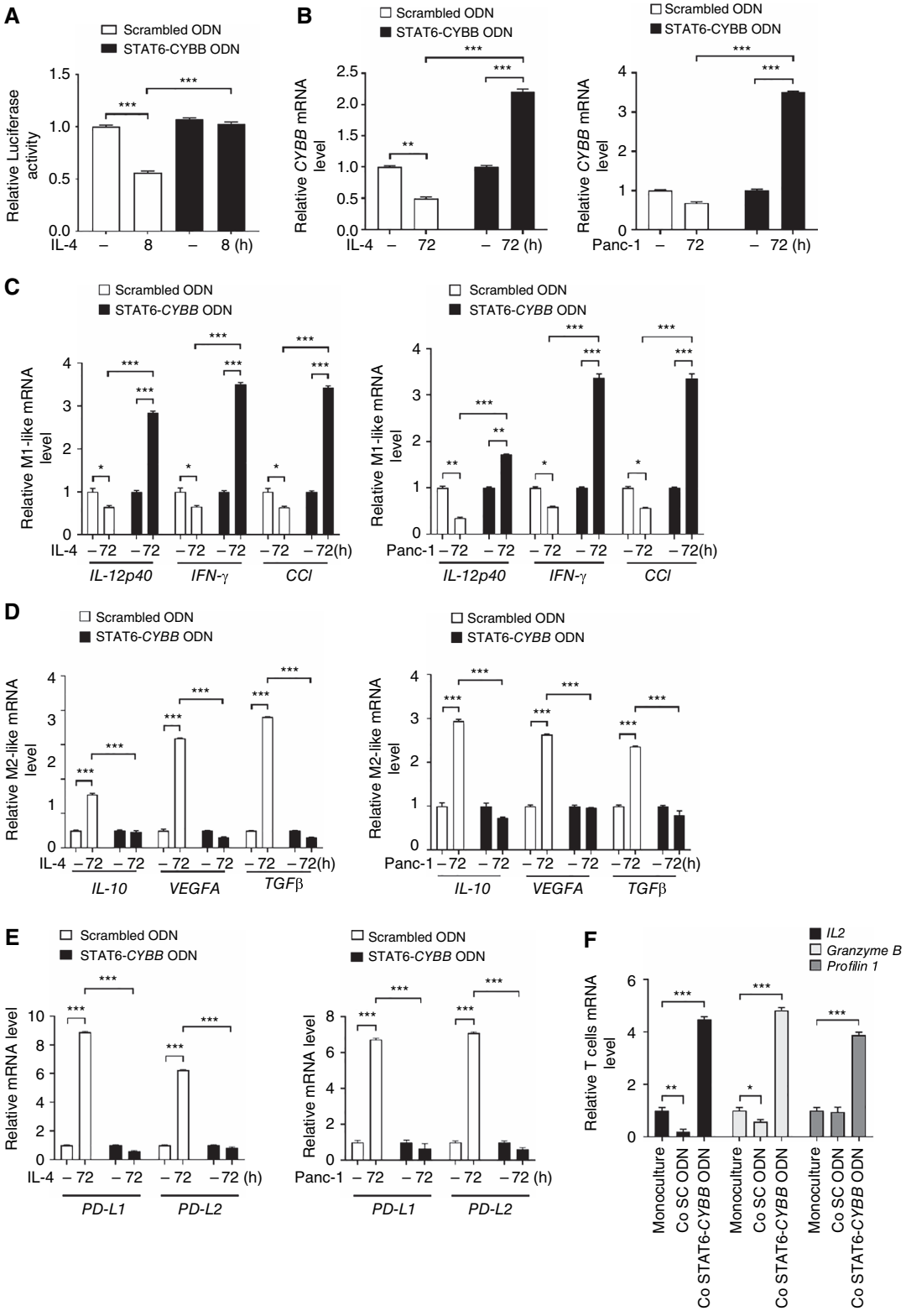

Figure 4.

STAT6-*CYBB* ODNs trapping STAT6 repress CYBB transcription to prevent M2-like polarization. **A,** After 24 hours of transfection with the *CYBB*-WT and pRL-TK reporters, U937 cells were electroporated with the scrambled ODNs and STAT6-*CYBB* decoy ODNs (1 μg/mL) followed by treatment with IL4 (20 ng/mL) for 8 hours and then measurement of luciferase activity. The bar graphs depict relative luciferase activity. ***, $P < 0.001$, (*Continued on the following page.*)

during which the temperature was reduced from 90°C to 25°C. After annealing, the reaction mixture was maintained at 4°C.

Statistical analysis

Each experiment was performed at least three times independently under identical conditions, and the data are expressed as the mean ± standard error of the mean (SEM). Student *t* test and one-way ANOVA were used to analyze differences. Statistical analyses were performed using GraphPad Prism 9.0 (GraphPad Software Inc., La Jolla, CA, USA) and SigmaPlot 12.0 (Systat Software Inc.). Statistical probability (*P*) is expressed as ***, $P < 0.001$; **, $P < 0.01$; *, $P < 0.05$.

Data availability

The authors confirm that the data supporting the findings of this study are available in the article and the supplementary information. Raw data supporting the findings of this study are available for the corresponding author upon reasonable request.

Results

Downregulation of CYBB occurs in M2-like macrophages and confers poor prognosis

Previous studies have shown that monocytic U937 cells can polarize to M2-like macrophages in response to tumor-derived factors (40, 41). Using gene expression microarray analysis, we have identified the potential genes that contribute to macrophage polarization. Compared to LPS treatment that induced M1-like polarization as a control, 72 hours of coculture with PANC-1 cells led to significantly increased expression of M2-like macrophage markers but decreased expression of M1-like macrophage markers and ROS-associated CYBB in U937 cells (**Fig. 1A**). The microarray data were confirmed by qPCR (**Fig. 1B**). As CYBB expression was downregulated in M2-like macrophages, we sought to determine the clinical significance of CYBB. We assessed the correlation between *CYBB* expression and the M2-like/M1-like ratio from our RNA-seq data (FPKM values) of 100 pancreatic tumors. A significantly negative correlation between *CYBB* expression and the M2-like/M1-like ratio was observed ($r = -0.269$, $P = 0.0068$; **Fig. 1C**), and the clinicopathological characteristics of these patients are shown in Supplementary Table S3. Next, we performed IF staining for CYBB on 180 human pancreatic cancer TMAs. The clinicopathological characteristics of these patients are shown in Supplementary Table S4. After quantification of the area percentages of staining, we found that pancreatic tumor tissues had lower CYBB expression than unpaired or paired normal tissues (**Fig. 1D**). We further divided the patients into the $CYBB^{Low}$ group (staining percentage <50%) and the $CYBB^{High}$ group (staining percentage ≥50%, Supplementary Fig. S1A). The $CYBB^{Low}$ group showed significantly worse overall survival (OS; $P = 0.002$, Supplementary Fig. S1B) and disease-free survival (DFS; $P < 0.001$, Supplementary Fig. S1C) than the $CYBB^{High}$ group, consistent with the data showing that patients with high CD204 M2-like expression also had shorter OS ($P = 0.057$, Supplementary Fig. S1D) and DFS ($P = 0.217$, Supplementary Fig. S1E). Furthermore, the combination of $CYBB^{Low}$ and $CD204^{High}$ M2-like conferred the worst OS ($P < 0.001$, **Fig. 1E**) and DFS ($P = 0.018$, **Fig. 1F**). Taken together, these results indicate that CYBB is a key regulator of M2-like macrophages polarization and is associated with worst patient survival.

ROS produced by CYBB is essential for IL4/STAT6-mediated M2-like polarization

IL4 can promote the proliferation and survival of cancer cells and is a key inducer of M2-like polarization (42). During the coculture with U937 cells, expression of *IL4* mRNA was increased in various pancreatic cancer cell lines (**Fig. 1G**), and the expression of IL4 protein was increased in U937 cells cocultured with PANC-1 cells at a time-dependent manner (Supplementary Fig. S2). However, at 72 hours after coculture, blockade of IL4 signaling with neutralizing antibodies reversed the downregulation of *CD86* and *CYBB* mRNA levels but suppressed *CD204, MRC1 (CD206)*, and *ARG1* mRNA expression in U937 cells (**Fig. 1H**; Supplementary Fig. S3). Similarly, CD86 protein expression was increased but CD204 protein expression was reduced by addition of IL4 neutralizing antibodies (**Fig. 1I**). These data indicated the importance of IL4 for M2-like polarization. Furthermore, we also found that *CYBB* mRNA expression was decreased by IL4 treatment in both U937 cells and mouse BMDMs (**Fig. 1J**), suggesting that CYBB expression can be regulated by IL4. As STAT6 is a key mediator of macrophage polarization and a major downstream effector of the IL4 pathway, we next investigated the involvement of STAT6 in IL4-mediated CYBB downregulation. After treatment with IL4, STAT6 and its upstream kinases JAK1 and JAK3 were phosphorylated, followed by a decrease in CYBB expression at 8 to 24 hours (**Fig. 2A**). As ROS have been reported to play an important role in TAMs differentiation, we also examined whether ROS contribute to the effect of IL4. Interestingly, after pretreatment with DPI (43), a flavoenzyme inhibitor that inhibited CYBB activity, to attenuate ROS production, IL4-induced phosphorylation of JAK1, JAK3, and STAT6 in U937 cells was significantly suppressed (**Fig. 2B**), suggesting that ROS produced by CYBB are required for IL4-mediated M2 polarization. In addition, pharmacological inhibition of JAK1, JAK3, and STAT6 restored IL4-mediated downregulation of CYBB, suggesting that IL4 reduces CYBB expression to promote M2-like polarization through STAT6 activation (**Fig. 2C**). To study whether ROS alone are sufficient to induce M2-like polarization, we added hydrogen peroxide (H_2O_2) to generate ROS in U937 cells. After treatment with H_2O_2, the phosphorylation of JAK1, JAK3, and STAT6 and expression of CYBB did not significantly change (Supplementary Fig. S4). However, cotreatment with IL4 and H_2O_2 could significantly induce CD204 expression and the phosphorylation of JAK1, JAK3, and STAT6 (**Fig. 2D**). Taken together, these results indicate that ROS plays an essential role in regulating the activation of the IL4/JAK/STAT6 pathway.

(*Continued*.) significant differences between groups. Next, U937 cells were electronically transfected with scrambled ODNs and STAT6-*CYBB* decoy ODNs followed by treatment with IL4 (20 ng/mL). **B,** RT-qPCR analysis of *CYBB* expression was performed. The bar graphs depict relative mRNA expression. **, $P < 0.01$; ***, $P < 0.001$, compared with control. Data represent the mean of three independent experiments. **C–E,** After IL4 treatment (20 ng/mL) or cocultured with PANC-1 cells, RT-qPCR analysis for M1-like markers (*IL12p40*, *IFNγ*, and *CCL2*), the M2-like markers (*IL10*, *VEGFA*, and *TGFβ*), the immune checkpoint proteins (*PD-L1* and *PD-L2*) was performed in U937 cells. The bar graphs depict relative mRNA expression. *, $P < 0.05$; ***, $P < 0.001$, compared with control. Data represent the mean of three independent experiments. **F,** After scrambled ODN (SC-ODN) and STAT6-*CYBB* ODN treatment, macrophages were cocultured with PANC-1 cells for 72 hours. PANC-1 cells–polarized SC ODN macrophages or STAT6-*CYBB* ODN macrophages were then cocultured with Jurkat cells for 72 hours, and RT-qPCR analysis of *IL2*, *Granzyme B*, and *Profilin 1* gene expression in Jurkat cells was performed. The bar graphs depict relative mRNA expression. **, $P < 0.05$; **, $P < 0.01$; ***, $P < 0.001$. Data represent the mean of three independent experiments.

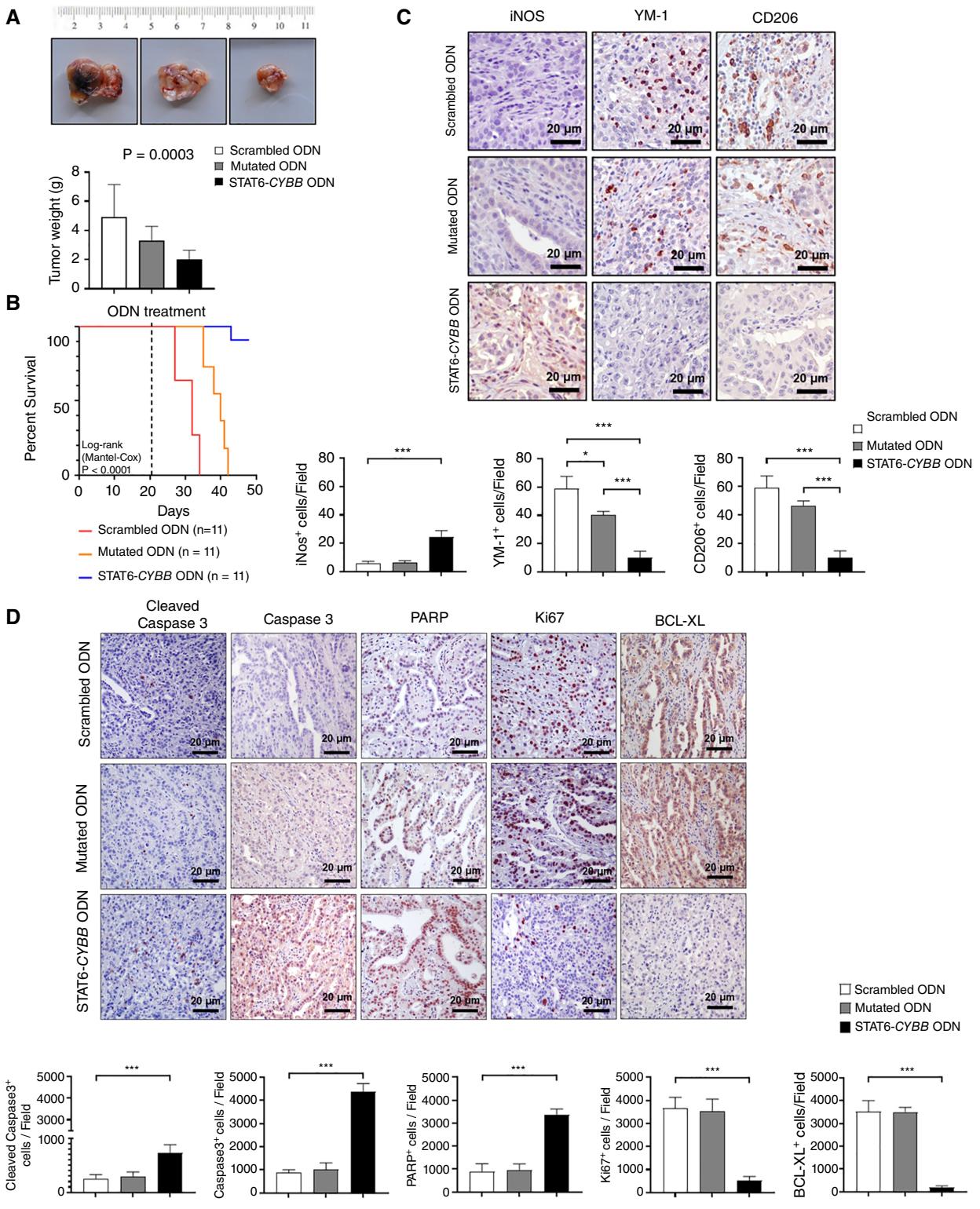

Figure 5.

STAT6-*CYBB* decoy ODNs slow pancreatic tumor growth. **A,** After 3 weeks of intravenous injection with decoy ODN (1 μg/mL), tumor weight was measured and compared between the scrambled ODN group, the mutated ODN group, and the STAT6-*CYBB* ODN group ($P = 0.0003$). **B,** Animal survival was compared between the three groups, scrambled ODN, mutated ODN, and STAT6-*CYBB* ODN ($P < 0.0001$ determined using the log-rank test). **C,** IHC staining for the M1-like marker (iNOS) and M2-like markers (CD206 and YM-1) was performed in KPC tumors from mice treated with scrambled (*Continued on the following page.*)

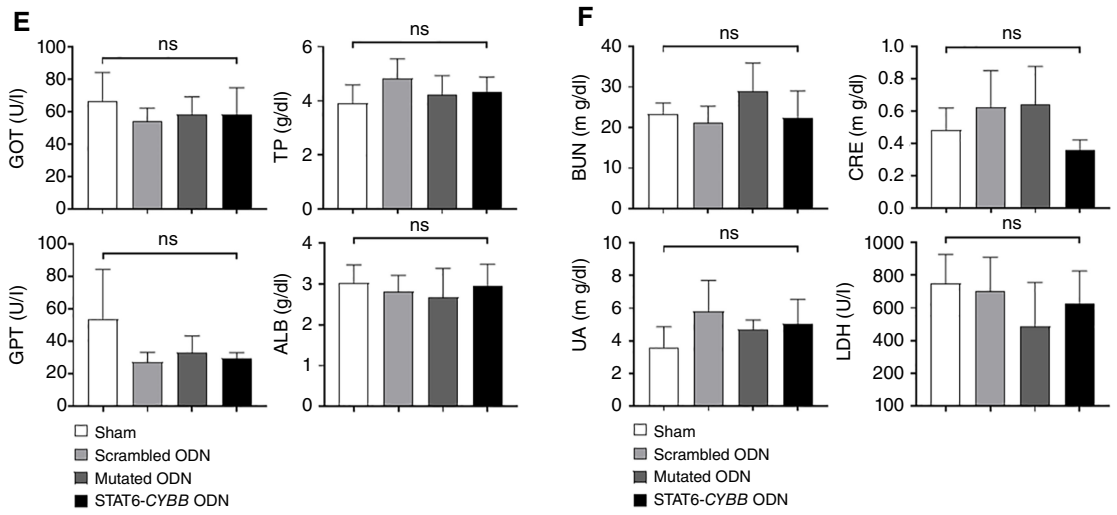

Figure 5.

(*Continued.*) ODN, mutated ODN, or the STAT6-*CYBB* ODN. The bar graphs depict the number of stained cells. *, $P < 0.05$; ***, $P < 0.001$, significant differences between groups. Five random fields of three random sections from each mouse were used to quantify the positive cells. **D,** IHC staining for the cell proliferation marker Ki67, the cell apoptosis markers cleaved caspase 3, caspase 3, and PARP, and the antiapoptosis marker BCL-XL was performed in KPC tumors treated with scrambled ODNs, mutated ODNs, and STAT6-*CYBB* ODNs. The bar graphs depict the numbers of stained cells/fields. Differences in the positively stained cell numbers between the three groups were compared. ***, $P < 0.001$. Five random fields of three random sections from each mouse were used to quantify the positive cells. **E,** Hepatotoxicity of decoy ODNs was determined by measuring GOT, GPT, ALB, and TP in mouse serum. **F,** Nephrotoxicity of decoy ODNs was determined by measuring BUN, UA, CRE, and LDH in mouse serum.

The IL4/STAT6 pathway upregulates HDAC2 to epigenetically reduce *CYBB* expression in M2-like TAMs

The epigenetic regulator HDAC modulates inflammatory responses in the TME and affects the polarization of M1-like/M2-like macrophages (44–46). In our microarray data, we found that *HDAC2* expression was increased in M2-like TAMs (**Fig. 2E**), suggesting that HDAC2 plays a role in M2-like polarization. Coculture with pancreatic cancer cells increased *HDAC2* mRNA expression in U937 cells and mouse BMDMs (**Fig. 2F**). Treatment with IL4 to activate STAT6 increased HDAC2 expression and decreased CYBB expression at the mRNA (Supplementary Fig. S5) and protein levels (**Fig. 2G**) in a time-dependent manner. Direct interactions between HDACs and STATs have been observed in previous research (47). By coimmunoprecipitation assay, there was a direct interaction between STAT6 and HDAC2 in U937 cells after IL4 treatment (**Fig. 2H**), suggesting that the two proteins cooperate to regulate *CYBB* transcription. Inhibiting STAT6 with AS1517499 and inhibiting HDAC2 with TSA or LBH589 reduced IL4-induced HDAC2 expression and restored IL4-mediated downregulation of CYBB at the mRNA (Supplementary Fig. S6) and protein levels (**Fig. 2I**). Similar results were also observed in the coculture experiments in which treatment with STAT6 and HDAC2 inhibitors restored the coculture-induced *CYBB* downregulation in U937 cells (Supplementary Fig. S7). Furthermore, RNAi targeting STAT6 and HDAC2 in U937 cells reduced M2-like polarization ($IL10^{High}$) and restored mRNA and protein expression of CYBB but did not affect M1-like polarization ($IL12p40^{High}$; Supplementary Fig. S8A–C; **Fig. 2J**). Similar results were also observed in the coculture experiments in which RNAi targeting STAT6 and HDAC2 reduced the coculture-induced M2-like polarization but did not affect M1-like polarization and restored the coculture-induced CYBB expression in U937 cells (Supplementary Fig. S9). The IL4/STAT6 signaling pathway was similar like in acute monocytic leukemia cell (THP-1; Supplementary Fig. S10). Collectively, these data indicate that HDAC2 functions as a key downstream regulator of IL4/STAT6 signaling to modulate M2-like polarization.

IL4-derived STAT6 interacted with the corepressor HDAC2 to bind to the *CYBB* promoter

To study how STAT6 and the corepressor HDAC2 regulate expression of *CYBB*, we performed ChIP assay to determine whether STAT6 and HDAC2 binds to the *CYBB* promoter. Several ChIP PCR primers were designed for the *CYBB* promoter, as shown in **Fig. 3A**. PCR products covering the D primer (−896/−719) region of the *CYBB* promoter were detected using ChIP-PCR and ChIP-QPCR after IL4 stimulation (**Fig. 3B** and **C**), suggesting a potential binding site for STAT6 and HDAC2 within the −896/−719 region. IL4 treatment triggered the binding of STAT6 to the promoter region, but this effect was inhibited by STAT6 knockdown (**Fig. 3B** and **C**). Taken together, these results indicate that IL4 stimulated the binding of STAT6 and HDAC2 to the *CYBB* promoter.

Next, we constructed the luciferase reporter plasmids with the WT *CYBB* promoter and mutated *CYBB* promoters in which the STAT6-binding sequence was changed (**Fig. 3D**). The reporter assay showed that IL4 decreased the luciferase activity of the WT *CYBB* promoter reporter but not that of the mutated *CYBB* promoter reporter (**Fig. 3E**). Silencing STAT6 effectively blocked the effect of IL4 (**Fig. 3E**). Taken together, these data suggest that IL4 from pancreatic cancer cells and ROS in macrophages can cooperate to activate STAT6 and HDAC2, and thus M2-like polarization, which contributes to the development of cold TME (noninflamed, immunologically ignorant) of pancreatic cancer (**Fig. 3F**).

STAT6-*CYBB* decoy ODNs impede the polarization of M2-like macrophages

TF decoy ODNs have been applied to interfere with the interaction between TFs and their corresponding genomic binding sites

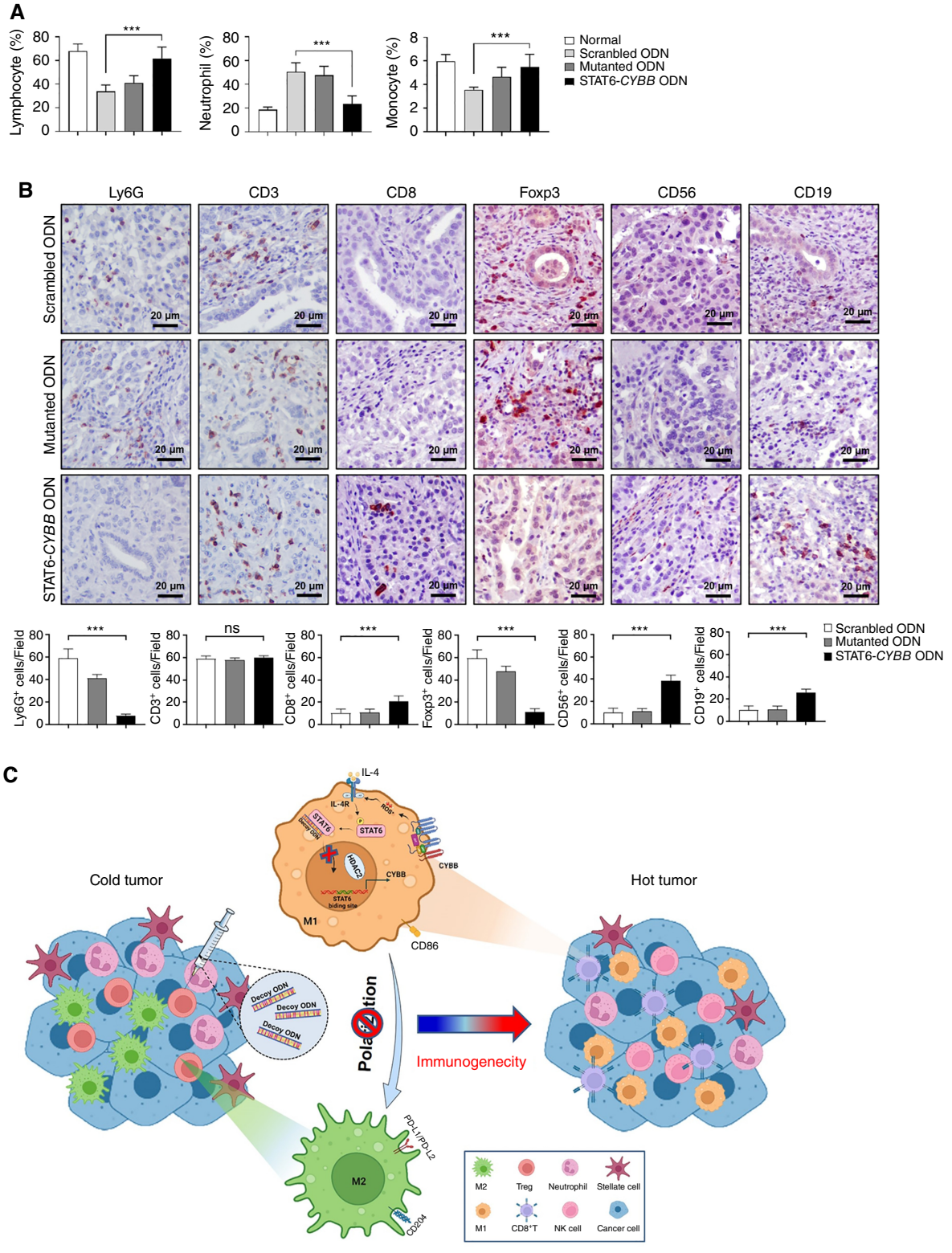

Figure 6.

STAT6-*CYBB* decoy ODNs enhance antitumor immune responses. **A,** Neutrophil, lymphocyte, and monocyte populations in blood circulation were analyzed using the complete blood count in mice of the scrambled ODN group, the mutated ODN group, and the STAT6-*CYBB* ODN group. The dot plots depict the cell percentages. **B,** IHC staining for the neutrophil marker Ly6G, the T-cell subpopulation markers CD3, CD8, and Foxp3, the (*Continued on the following page.*)

through competitive suppression, selectively regulating gene expression in cells as a therapeutic agent with great potential (28, 48). Therefore, we investigated whether decoy ODNs can inhibit the binding of STAT6 to the *CYBB* promoter and thus reduce M2-like polarization. A 28mer double-strand ODN was designed to inhibit STAT6 binding to the *CYBB* promoter. The reporter assay showed that IL4 treatment could repress CYBB expression by reducing its promoter activity; however, treatment with the STAT6-*CYBB* decoy ODN reversed the reduction of WT CYBB promoter-driven luciferase activity by IL4. (**Fig. 4A**). Furthermore, in U937 cells, the STAT6-*CYBB* decoy ODN also increased the expression of *CYBB* mRNA (**Fig. 4B**) and the expression of M1-like cytokines including *IL12p40*, *IFN*γ, and *CCL2*, but decreased the expression of M2-like cytokines including *IL10*, *VEGFA*, and *TGFβ1* after IL4 treatment (**Fig. 4C** and **D**) or coculture with PANC-1 cells (**Fig 4C** and **D**). Treatment with the STAT6-*CYBB* decoy ODN also decreased the mRNA expression of *PD-L1* and *PD-L2* in U937 cells in the presence of IL4 or when cocultured with PANC-1 cells (**Fig. 4E**). U937 cells treatment with the STAT6-*CYBB* decoy ODN after coculturing with PANC-1 cells also increased the mRNA expression of *IL2*, *Granzyme B*, and *Profilin 1* in the Jurkat T cells (**Fig. 4F**), thereby increasing the proliferation of Jurkat T cells and $\alpha CD3^+$ PBMC cells in the CFSE assay (Supplementary Fig. S11). These results suggest that STAT6-*CYBB* decoy ODNs can significantly prevent the formation of M2-like TAMs, increase T-cell proliferation, and have the potential as an effective therapeutic approach for pancreatic cancer.

STAT6-*CYBB* decoy ODNs slow tumor growth and counteracts immunosuppression

Because STAT6-*CYBB* decoy ODNs effectively impeded the formation of M2-like macrophages *in vitro*, we evaluated the therapeutic effects of STAT6-*CYBB* decoy ODNs on pancreatic cancer *in vivo*. Twenty days after the inoculation of KPC^{LUC} cells into the pancreas, mice were intravenously injected with scrambled ODNs, STAT6-*CYBB* decoy ODNs, and mutated STAT6-*CYBB* decoy ODNs. Three weeks after treatment with decoy ODNs, the mice were sacrificed to collect tumors. Mice treated with STAT6-*CYBB* decoy ODNs had the lowest tumor volume and tumor weight ($P = 0.0003$; **Fig. 5A**). In addition, compared with scrambled ODNs and mutated STAT6-*CYBB* decoy ODNs, STAT6-*CYBB* decoy ODNs significantly extended the survival of pancreatic tumor-bearing mice ($P < 0.0001$; **Fig. 5B**). Immunohistochemistry (IHC) staining showed that STAT6-*CYBB* decoy ODNs significantly increased the expression of iNOS and CYBB but reduced the expression of CD206 and YM-1 (**Fig. 5C**; Supplementary Fig. 12). Compared to the tumors receiving scrambled or mutated decoy ODNs, the STAT6-*CYBB* decoy ODNs group exhibited increased expression of caspase 3, cleaved caspase 3, and PARP, and decreased expression of the antiapoptotic marker BCL-XL and the cell proliferation marker ki67 (**Fig. 5D**), suggesting that STAT6-*CYBB* decoy ODNs reduced pancreatic tumor growth by promoting cell apoptosis and suppressing cell proliferation. Therefore, treatment with STAT6-CYBB ODN also suppresses stromal or epithelial-type cell activation (Supplementary Fig. S13). Serum levels of glutamic oxaloacetic transaminase (GOT), glutamic pyruvic transaminase (GPT), albumin (ALB), and total protein (TP) for liver function monitoring (**Fig. 5E**) and the serum levels of blood urea nitrogen (BUN), uric acid (UA), creatinine (CRE), and lactate dehydrogenase (LDH) for renal function monitoring (**Fig. 5F**) in mice were not affected by decoy ODNs compared with sham treatment.

Compared with scrambled and mutated decoy ODNs, STAT6-*CYBB* decoy ODNs also decreased neutrophil levels but increased lymphocyte and monocyte percentages in the blood circulation (**Fig. 6A**). In tumors, STAT6-*CYBB* decoy ODNs downregulated the neutrophil marker Ly6G and the regulatory T-cell marker Foxp3 but upregulated the total lymphocyte marker CD3, the cytotoxic T marker CD8, the NK-cell marker CD56, and the B-cell marker CD19 (**Fig. 6B**). Moreover, we also confirmed that the cytotoxic marker Granzyme B was upregulated in tumors treated with STAT6-*CYBB* ODN (Supplementary Fig. S14). These results indicate that STAT6-*CYBB* decoy ODNs without toxicity have great potential to inhibit M2-like polarization and thus reduce immunosuppression and pancreatic cancer growth (**Fig. 6C**).

Discussion

A high density of M2-like macrophages in the pancreatic TME confers poor prognosis. Interrupting the polarization of M2-like TAMs is a potential strategy for pancreatic cancer therapy. Here, we showed that cancer cell-derived IL4 in combination with ROS to activate STAT6/HDAC2 in macrophages could repress *CYBB* transcription and skew M2-like in the TME of pancreatic cancer. STAT6-*CYBB* decoy ODNs blocked STAT6/HDAC2 binding to the *CYBB* promoted and prevented M2-like polarization. This action can maintain the transcription of *CYBB* to produce ROS, thus maintaining the M1-like phenotype in macrophages and reactivating antitumor immunity to attack cancer cells. Our preclinical animal study provided strong evidence that gene therapy of STAT6-*CYBB* decoy ODNs could effectively turn "cold" tumors into "hot" ones by inhibiting the formation of M2-like TAMs and upregulating antitumor immune responses in pancreatic TME.

As a multifunctional cytokine in the TME, IL4 not only participates in alternative macrophage priming but also accelerates pancreatic cancer progression (49). By binding to IL4R or IL13R, IL4 activates STAT6 signaling to polarize macrophages to the M2-like phenotype; however, the detailed mechanism has not been fully elucidated (50). It has been reported that IL4 stimulates STAT6 activation and the upregulation of immunoglobulin heavy chain via histone modification in B-cell differentiation, suggesting the involvement of epigenetic regulation in IL4 signaling–associated cell differentiation (51). Consistently, our results showed that IL4 promoted M2-like polarization by upregulating HDAC2 to diminish *CYBB* gene expression.

Previously, HDAC inhibitors have been reported to inhibit inflammation and promote M2-like macrophage formation (45); however, the underlying mechanism is unclear. Our microarray analysis showed that the expression of HDAC2 was increased in U937 cells after coculture with PANC-1 cells. Furthermore, we demonstrated that the cooperation of IL4 with *CYBB*-derived ROS strongly activated the STAT6/HDAC2 pathway to inhibit *CYBB*

(*Continued.*) NK-cell marker CD56, and the **B** cell marker CD19 was performed in KPC tumors from the scrambled ODN, mutated ODN, and STAT6-*CYBB* ODN–treated mice. The bar graphs depict the numbers of stained cells/fields. Differences in the positively stained cell numbers between the three groups were compared. *, $P < 0.05$; ***, $P < 0.001$. Five random fields of three random sections from each mouse were used to quantify the positive cells. **C,** Schematic conclusion showing the gene therapy of STAT6-*CYBB* decoy ODNs is a promising therapeutic strategy to convert immunologically cold tumors into hot tumors by preventing M2-like polarization.

gene transcription, thus promoting the formation of M2-like. During the conversion of the M1-like phenotype to the M2-like phenotype, *CYBB* is critical at the beginning because of its function in ROS production; however, after M2-like formation, *CYBB* function is suppressed, suggesting that *CYBB*-derived ROS are not necessary for M2-like function and their maintenance.

Previous studies have shown that decoy ODNs focusing on myc-associated zinc finger and high mobility group AT-hook 1 (HMGA-1) inhibit the activation of *KRAS* transcription and HMGA-1-associated gemcitabine resistance in pancreatic cancer, respectively (52, 53). Additionally, a recent clinical trial has investigated the treatment effectiveness of STAT3 decoy ODNs in head and neck cancer (27). The decoy of TFs provides a novel strategy for interrupting gene expression and has several substantive advantages over knockout animal studies. In other words, decoy ODN have been recognized as an important tool in gene therapy for accurately targeting human diseases. Our study showed that the use of STAT6-*CYBB* decoy ODNs could markedly suppress M2-like polarization and reduce pancreatic tumor growth. Furthermore, no obvious hepatotoxicity or nephrotoxicity was observed in treated mice.

In conclusion, we clearly demonstrated that, in the TME of pancreatic cancer, cancer cells secrete IL4 to skew M2-like polarization via activation of CYBB-ROS/STAT6/HDAC2 signaling in macrophages. Treatment with STAT6-*CYBB* decoy ODNs can block M2-like formation to enhance antitumor immune responses in the TME and reduce tumor growth, suggesting a novel gene therapy tool for the treatment of pancreatic cancer.

Authors' Disclosures

C.-J. Chen reports grants from National Science and Technology Council, R.O.C during the conduct of the study. H.-C. Wang reports grants from National Science and Technology Council, R.O.C during the conduct of the study. No disclosures were reported by the other authors.

Authors' Contributions

C.-J. Chen: Data curation, formal analysis, investigation, methodology, writing–original draft. **H.-C. Wang:** Data curation, formal analysis, supervision, investigation, writing–original draft. **Y.-C. Hou:** Conceptualization, data curation, supervision. **Y.-Y. Wu:** Data curation, investigation, methodology. **C.-C. Shieh:** Conceptualization, resources, supervision, writing–review and editing. **Y.-S. Shan:** Conceptualization, resources, supervision, funding acquisition, project administration, writing–review and editing.

Ethics Approval and Consent to Participate

This study was approved by the Ethical Committee and Institutional Review Board of National Cheng Kung University Hospital (IRB number: A-ER-105-459) and the Institutional Animal Care and Use Committee of National Cheng Kung University (IACUC NO.:103150 and of 110331).

Consent for Publication

All the authors in the study have consented to publish this paper.

Acknowledgments

We are grateful for technical support from 1. Human Biobank, 2. Immunobiology Core, 3. Flow Cytometry Core Facilities, Clinical Medicine Research Center, National Cheng Kung University Hospital, and technical support from the Laboratory Animal Center, College of Medicine, National Cheng Kung University, and Taiwan Animal Consortium. This study was supported by the National Cheng Kung University Hospital (grant number NCKUH-10301002) and the Ministry of Science and Technology, Taiwan (MOST 106-2314-B-006 -059; MOST 107-2314-B-006 -004; MOST 108-2314-B-006 -001).

Note

Supplementary data for this article are available at Molecular Cancer Therapeutics Online (http://mct.aacrjournals.org/).

Received November 3, 2023; revised February 29, 2024; accepted June 18, 2024; published first June 22, 2024.

References

1. Hanahan D, Weinberg RA. Hallmarks of cancer: the next generation. Cell 2011;144:646–74.
2. Bejarano L, Jordão MJC, Joyce JA. Therapeutic targeting of the tumor microenvironment. Cancer Discov 2021;11:933–59.
3. Ullman NA, Burchard PR, Dunne RF, Linehan DC. Immunologic strategies in pancreatic cancer: making *cold* tumors *hot*. J Clin Oncol 2022;40:2789–805.
4. Liu Y-T, Sun Z-J. Turning cold tumors into hot tumors by improving T-cell infiltration. Theranostics 2021;11:5365–86.
5. Jang H-J, Lee H-S, Yu W, Ramineni M, Truong CY, Ramos D, et al. Therapeutic targeting of macrophage plasticity remodels the tumor-immune microenvironment. Cancer Res 2022;82:2593–609.
6. Anderson NM, Simon MC. The tumor microenvironment. Curr Biol 2020;30:R921–5.
7. Locati M, Curtale G, Mantovani A. Diversity, mechanisms, and significance of macrophage plasticity. Annu Rev Pathol 2020;15:123–47.
8. Ricketts TD, Prieto-Dominguez N, Gowda PS, Ubil E. Mechanisms of macrophage plasticity in the tumor environment: manipulating activation state to improve outcomes. Front Immunol 2021;12:642285.
9. Jayasingam SD, Citartan M, Thang TH, Mat Zin AA, Ang KC, Ch'ng ES. Evaluating the polarization of tumor-associated macrophages into M1 and M2 phenotypes in human cancer tissue: technicalities and challenges in routine clinical practice. Front Oncol 2020;9:1512.
10. Genard G, Lucas S, Michiels C. Reprogramming of tumor-associated macrophages with anticancer therapies: radiotherapy versus chemo- and immunotherapies. Front Immunol 2017;8:828.
11. Chen Y, Song Y, Du W, Gong L, Chang H, Zou Z. Tumor-associated macrophages: an accomplice in solid tumor progression. J Biomed Sci 2019;26:78.
12. Pan Y, Yu Y, Wang X, Zhang T. Tumor-associated macrophages in tumor immunity. Front Immunol 2020;11:583084.
13. Mehraj U, Qayoom H, Mir MA. Prognostic significance and targeting tumor-associated macrophages in cancer: new insights and future perspectives. Breast Cancer 2021;28:539–55.
14. Hensler M, Kasikova L, Fiser K, Rakova J, Skapa P, Laco J, et al. M2-like macrophages dictate clinically relevant immunosuppression in metastatic ovarian cancer. J Immunother Cancer 2020;8:e000979.
15. Zhu Z, Zhang H, Chen B, Liu X, Zhang S, Zong Z, et al. PD-L1-mediated immunosuppression in glioblastoma is associated with the infiltration and M2-polarization of tumor-associated macrophages. Front Immunol 2020;11:588552.
16. Ferrari CKB, Souto PCS, França EL, Honorio-Franca AC. Oxidative and nitrosative stress on phagocytes' function: from effective defense to immunity evasion mechanisms. Arch Immunol Ther Exp (Warsz) 2011;59:441–8.
17. Nauseef WM. Nox enzymes in immune cells. Semin Immunopathol 2008;30:195–208.
18. Brandes RP, Weissmann N, Schröder K. Nox family NADPH oxidases: molecular mechanisms of activation. Free Radic Biol Med 2014;76:208–26.
19. Zhang Y, Choksi S, Chen K, Pobezinskaya Y, Linnoila I, Liu Z-G. ROS play a critical role in the differentiation of alternatively activated macrophages and the occurrence of tumor-associated macrophages. Cell Res 2013;23:898–914.
20. Hosein AN, Dougan SK, Aguirre AJ, Maitra A. Translational advances in pancreatic ductal adenocarcinoma therapy. Nat Cancer 2022;3:272–86.
21. Sedighzadeh SS, Khoshbin AP, Razi S, Keshavarz-Fathi M, Rezaei N. A narrative review of tumor-associated macrophages in lung cancer: regulation of macrophage polarization and therapeutic implications. Transl Lung Cancer Res 2021;10:1889–916.

22. Schweer D, McAtee A, Neupane K, Richards C, Ueland F, Kolesar J. Tumor-associated macrophages and ovarian cancer: implications for therapy. Cancers (Basel) 2022;14:2220.
23. Tu MM, Abdel-Hafiz HA, Jones RT, Jean A, Hoff KJ, Duex JE, et al. Inhibition of the CCL2 receptor, CCR2, enhances tumor response to immune checkpoint therapy. Commun Biol 2020;3:720.
24. Fei L, Ren X, Yu H, Zhan Y. Targeting the CCL2/CCR2 Axis in cancer immunotherapy: one stone, three birds? Front Immunol 2021;12:771210.
25. Noel M, O'Reilly EM, Wolpin BM, Ryan DP, Bullock AJ, Britten CD, et al. Phase 1b study of a small molecule antagonist of human chemokine (C-C motif) receptor 2 (PF-04136309) in combination with nab-paclitaxel/gemcitabine in first-line treatment of metastatic pancreatic ductal adenocarcinoma. Invest New Drugs 2020;38:800–11.
26. Leong PL, Andrews GA, Johnson DE, Dyer KF, Xi S, Mai JC, et al. Targeted inhibition of Stat3 with a decoy oligonucleotide abrogates head and neck cancer cell growth. Proc Natl Acad Sci U S A 2003;100:4138–43.
27. Sen M, Thomas SM, Kim S, Yeh JI, Ferris RL, Johnson JT, et al. First-in-human trial of a STAT3 decoy oligonucleotide in head and neck tumors: implications for cancer therapy. Cancer Discov 2012;2:694–705.
28. Tehran MM, Rezaei S, Jalili A, Aghaee-Bakhtiari SH, Sahebkar A. Decoy oligodeoxynucleotide technology: an emerging paradigm for breast cancer treatment. Drug Discov Today 2020;25:195–200.
29. Wang M, Zhang Z, Zhang W. Design, synthesis, and application of chiral bicyclic imidazole catalysts. Acc Chem Res 2022;55:2708–27.
30. Bertani B, Ruiz N. Function and biogenesis of lipopolysaccharides. EcoSal Plus 2018;8.
31. Dimitrova P, Skapenko A, Herrmann ML, Schleyerbach R, Kalden JR, Schulze-Koops H. Restriction of de novo pyrimidine biosynthesis inhibits Th1 cell activation and promotes Th2 cell differentiation. J Immunol 2002;169:3392–9.
32. Chen W, Sivaprasad U, Tabata Y, Gibson AM, Stier MT, Finkelman FD, et al. IL-13R alpha 2 membrane and soluble isoforms differ in humans and mice. J Immunol 2009;183:7870–6.
33. Yao L, Mustafa N, Tan EC, Poulsen A, Singh P, Duong-Thi M-D, et al. Design and synthesis of ligand efficient dual inhibitors of janus kinase (JAK) and histone deacetylase (HDAC) based on ruxolitinib and vorinostat. J Med Chem 2017;60:8336–57.
34. Verzijl GKM, Schuster C, Dax T, de Vries AHM, Lefort L. Asymmetric synthesis of a key intermediate for Tofacitinib via a dynamic kinetic resolution-reductive amination protocol. Org Process Res Dev 2018;22:1817–22.
35. Nagashima S, Yokota M, Nakai E-I, Kuromitsu S, Ohga K, Takeuchi M, et al. Synthesis and evaluation of 2-{[2-(4-hydroxyphenyl)-ethyl]amino}pyrimidine-5-carboxamide derivatives as novel STAT6 inhibitors. Bioorg Med Chem 2007;15:1044–55.
36. Chatterjee A, Richer J, Hulett T, Iska VBR, Wiest O, Helquist P. An efficient synthesis of (+/−)-trichostatic acid and analogues: a new route to (+/−)-trichostatin A. Org Lett 2010;12:832–4.
37. Fredenhagen A, Kittelmann M, Oberer L, Kuhn A, Kühnöl J, Délémonté T, et al. Biocatalytic synthesis and structure elucidation of cyclized metabolites of the deacetylase inhibitor panobinostat (LBH589). Drug Metab Dispos 2012;40:1041–50.
38. Crinelli R, Bianchi M, Gentilini L, Magnani M. Design and characterization of decoy oligonucleotides containing locked nucleic acids. Nucleic Acids Res 2002;30:2435–43.
39. Casas G, Perche F, Midoux P, Pichon C, Malinge J-M. DNA minicircles as novel STAT3 decoy oligodeoxynucleotides endowed with anticancer activity in triple-negative breast cancer. Mol Ther Nucleic Acids 2022;29:162–75.
40. Chimal-Ramírez GK, Espinoza-Sánchez NA, Chávez-Sánchez L, Arriaga-Pizano L, Fuentes-Pananá EM. Monocyte differentiation towards protumor activity does not correlate with M1 or M2 phenotypes. J Immunol Res 2016;2016:6031486.
41. Little AC, Pathanjeli P, Wu Z, Bao L, Goo LE, Yates JA, et al. IL-4/IL-13 stimulated macrophages enhance breast cancer invasion via rho-GTPase regulation of synergistic VEGF/CCL-18 signaling. Front Oncol 2019;9:456.
42. Setrerrahmane S, Xu H. Tumor-related interleukins: old validated targets for new anti-cancer drug development. Mol Cancer 2017;16:153.
43. Scaife RM. Selective and irreversible cell cycle inhibition by diphenyleneiodonium. Mol Cancer Ther 2005;4:876–84.
44. Yang Q, Wei J, Zhong L, Shi M, Zhou P, Zuo S, et al. Cross talk between histone deacetylase 4 and STAT6 in the transcriptional regulation of arginase 1 during mouse dendritic cell differentiation. Mol Cell Biol 2015;35:63–75.
45. Mohammadi A, Sharifi A, Pourpaknia R, Mohammadian S, Sahebkar A. Manipulating macrophage polarization and function using classical HDAC inhibitors: implications for autoimmunity and inflammation. Crit Rev Oncol Hematol 2018;128:1–18.
46. Larionova I, Kazakova E, Patysheva M, Kzhyshkowska J. Transcriptional, epigenetic and metabolic programming of tumor-associated macrophages. Cancers (Basel) 2020;12:1411.
47. Czimmerer Z, Daniel B, Horvath A, Rückerl D, Nagy G, Kiss M, et al. The transcription factor STAT6 mediates direct repression of inflammatory enhancers and limits activation of alternatively polarized macrophages. Immunity 2018;48:75–90.e6.
48. Wang LH, Yang XY, Kirken RA, Resau JH, Farrar WL. Targeted disruption of stat6 DNA binding activity by an oligonucleotide decoy blocks IL-4-driven T(H)2 cell response. Blood 2000;95:1249–57.
49. Dey P, Li J, Zhang J, Chaurasiya S, Strom A, Wang H, et al. Oncogenic KRAS-driven metabolic reprogramming in pancreatic cancer cells utilizes cytokines from the tumor microenvironment. Cancer Discov 2020;10:608–25.
50. Guo M, Härtlova A, Gierliński M, Prescott A, Castellvi J, Losa JH, et al. Triggering MSR1 promotes JNK-mediated inflammation in IL-4-activated macrophages. EMBO J 2019;38:e100299.
51. Awosika O, Kim L, Mazhar M, Rengifo-Pardo M, Ehrlich A. Profile of dupilumab and its potential in the treatment of inadequately controlled moderate-to-severe atopic dermatitis. Clin Cosmet Investig Dermatol 2018;11:41–9.
52. Cogoi S, Zorzet S, Rapozzi V, Géci I, Pedersen EB, Xodo LE. MAZ-binding G4-decoy with locked nucleic acid and twisted intercalating nucleic acid modifications suppresses KRAS in pancreatic cancer cells and delays tumor growth in mice. Nucleic Acids Res 2013;41:4049–64.
53. Liau S-S, Whang E. HMGA1 is a molecular determinant of chemoresistance to gemcitabine in pancreatic adenocarcinoma. Clin Cancer Res 2008;14:1470–7.